https://doi.org/10.5194/egusphere-2025-4820
Preprint. Discussion started: 21 October 2025

The influence of vapor pressure deficit changes on global terrestrial evapotranspiration

Yuxin Miao[1,2,4], Guofeng Zhu[1,2,3,4*], Yuhao Wang[1,2,3,4], Enwei Huang[1,2,3,4], Qingyang Wang[1,2,4], Yani Gun[1,2,4], Zhijie Zheng[1,2,4], Jiangwei Yang[1,2,3], Wenmin Li[1,2,3], Ziwen Liu[1,2,3]

[1].College of Geography and Environmental Science, Northwest Normal University, Lanzhou 730070, Gansu, China

[2].Comprehensive Observatory of Ecological Environment in Shiyang River Basin, Northwest Normal University, Lanzhou, 730070, Gansu, China

[3].Gansu Key Laboratory of Oasis Resource Environment and Sustainable Development, Lanzhou, 730070, Gansu, China

[4].Remote Sensing Application Center of Ministry of Agriculture and Rural Affairs, Lanzhou Branch, Lanzhou, 730070, Gansu, China

[*] Correspondence to: Guofeng Zhu (zhugf@nwnu.edu.cn)

Abstract: Vapor pressure deficit (VPD) is increasingly recognized as the primary driver of uncertainty in future global evapotranspiration (E) trends. Accurately characterizing the spatiotemporal dynamics of VPD and clarifying its mechanisms of influence on terrestrial E are crucial for improving water-use efficiency, optimizing ecosystem structure and function, and addressing the challenges of global climate change. Previous studies, however, have largely concentrated on the physiological regulation of vegetation transpiration (Et) at the micro scale. Here, we integrate multi-source remote sensing products and reanalysis datasets spanning 1981–2020 to quantitatively disentangle the contributions of VPD to E and assess its role in shaping global terrestrial evapotranspiration. Our results demonstrate that: (1) across 60.7% of the global land surface, E increased with rising VPD, while in arid regions with limited soil moisture the effect was generally weak; (2) VPD regulates E primarily by modulating Et, with elevated VPD directly enhancing transpiration; (3) the regulation of E by VPD exhibits a clear climatic gradient: arid zones (1.31 kPa) > humid zones (0.32 kPa), and the tropical (0.79 kPa) > temperate (0.68 kPa) > cold (0.28 kPa) >

https://doi.org/10.5194/egusphere-2025-4820
Preprint. Discussion started: 21 October 2025

polar (0.07 kPa). By elucidating the dominant pathways and regional heterogeneity of VPD–E interactions at the global scale, this study strengthens the mechanistic understanding of the coupled warming–atmospheric aridity–water flux system. These findings provide quantitative constraints for predicting terrestrial water-cycle changes under global warming and offer scientific evidence to support targeted climate adaptation strategies worldwide.

Key words: Vapor pressure deficit; Evapotranspiration; Ecosystem; Climate change

1. Introduction

Vapor Pressure Deficit (VPD) is rising at an unprecedented rate and has become one of the core variables driving land drying and vegetation moisture stress under climate warming (Hermann et al., 2024). As a combined measure of temperature and relative humidity (Shih et al., 2025), the increase of VPD directly reflects the stronger atmospheric demand for water, which in turn strongly influences stomatal conductance, photosynthetic rate, and vegetation evapotranspiration (Chai et al., 2025; Miner et al., 2017). Many studies have shown that VPD has become a key variable linking the carbon–water cycle, ecosystem water use efficiency, and extreme climate events such as heat waves and droughts (Hermann et al., 2024). Under global warming, terrestrial ecosystems are facing “dual stress”: on the one hand, rising VPD intensifies water shortage; on the other hand, traditional climate models struggle to reproduce its nonlinear feedbacks, thereby creating substantial uncertainty in predicting future carbon–water cycle trends (Kim and Johnson, 2025). Therefore, a clear understanding of how VPD changes regulate global evapotranspiration is not only of scientific value but also of great practical significance for ecosystem adaptation to climate change.

Although higher global CO_2 concentrations should theoretically improve vegetation water use efficiency (WUE) (Peters et al., 2018), recent studies combining FLUXNET flux observations with machine learning have shown that global WUE has tended to level off since 2000. This slowdown is mainly due to the “asymmetric effect” of VPD on photosynthesis and evapotranspiration (ET)—while VPD promotes ET, it suppresses carbon assimilation, thus offsetting the CO_2 fertilization effect (F. Li et al.,

https://doi.org/10.5194/egusphere-2025-4820
Preprint. Discussion started: 21 October 2025

2023). In non-peatland areas, higher VPD generally limits vegetation growth and reduces carbon sink capacity. However, in high-water-level environments such as peatlands, this effect may be weakened or even reversed by the "open water strategy" (Chen et al., 2023; Yuan et al., 2019). Together, these findings highlight that VPD is not only a driver of ET but also an important regulator in the carbon–water coupling process. Yet, the spatial differences in the global VPD–ET relationship and its driving mechanisms remain poorly understood, and the specific pathways through which VPD operates under multi-factor interactions are still unclear.

In recent years, empirical research on the relationship between VPD and evapotranspiration has steadily expanded. At the microscopic scale, there is a daily lag between vegetation transpiration and VPD, with the size of the lag depending on the radiation–VPD delay. Both plant and soil water potential are key factors regulating this lagged ET–VPD relationship, especially when soil moisture declines (Zhang et al., 2014). At the macroscopic scale, in arid regions, the persistent rise in VPD combined with soil drought restricts evapotranspiration, causing vegetation wilting and ecosystem degradation (Wang et al., 2025). By contrast, in tropical rainforests where soil water is relatively abundant, although higher VPD induces stomatal closure, leaf renewal during the dry season can boost short-term carbon sequestration (Kumagai et al., 2009; Lebrija-Trejos et al., 2023). These contrasting responses indicate that the influence of VPD on evapotranspiration is shaped by climate zones, soil water availability, vegetation types, and even human activities (Zhuang et al., 2021). Therefore, understanding the nonlinearities, threshold effects, and multi-factor interactions in this relationship has become a major challenge in Earth system science (Hsu and Dirmeyer, 2021). Although some studies have tried to explain this relationship using statistical or process-based models, the lack of quantitative identification of VPD pathways remains a key limitation for improving predictive capability.

Against this background, this study explores how VPD influences evapotranspiration across different land surfaces and climate zones worldwide. Specifically, we used VPD and ET data derived from multiple remote sensing sources

https://doi.org/10.5194/egusphere-2025-4820
Preprint. Discussion started: 21 October 2025

to examine the global response of ET to VPD changes from 1981 to 2020. The research focuses on the following scientific questions: (1) How does VPD influence global terrestrial ET? (2) How does VPD affect the spatial and temporal heterogeneity of global ET? (3) What are the implications of the rapid rise of VPD under global warming for land–atmosphere feedbacks? Addressing these questions will not only improve our understanding of the mechanisms by which VPD regulates ET but also provide a stronger basis for developing targeted global climate adaptation strategies.

2. Data and Methods

2.1 Data Sources

Evapotranspiration data used in this study were derived from the Global Land Evaporation Amsterdam Model (GLEAM) v4.2a product (https://www.gleam.eu/) (Miralles et al., 2025). The GLEAM product not only provides total evapotranspiration but also partitions components such as transpiration (Et), bare soil evaporation (Eb), and interception evaporation (Ei), and is widely applied in quantitative global water cycle research. VPD data were obtained from the monthly ERA5 reanalysis available from the official website, with calculations based on air temperature (Ta) and dew point temperature (Td). Precipitation data were also analyzed on a monthly scale using ERA5. Other variables, including soil moisture, total solar radiation, and precipitation, were sourced from ERA5 as well (Copernicus Climate Change Service, 2019). Land use data were obtained from the MCD12C1 version 6.1 product on the Google Earth Engine platform, classifying land use into 17 categories at a spatial resolution of 0.05° annually (Friedl and Sulla-Menashe, 2022). Climate zoning employed the updated Köppen–Geiger classification system by Rubel et al. to define climate types for each region (Rubel et al., 2017). Arid regions are primarily distributed between 60°N and 60°S and are classified using the aridity index into hyper-arid, arid, semi-arid, and dry sub-humid zones (Rohde et al., 2024). Leaf Area Index (LAI) data were sourced from the GIMMS V1.2 dataset published in 2023 (Cao et al., 2023), which demonstrates high overall accuracy and low underestimation, validated by in situ LAI measurements and Landsat-derived LAI samples. This dataset effectively mitigates satellite orbit drift and sensor degradation effects,

https://doi.org/10.5194/egusphere-2025-4820
Preprint. Discussion started: 21 October 2025

providing good temporal consistency and a plausible global vegetation trend around the year 2000.

2.2 Methods

2.2.1 Trend analysis of raster data based on Theil-Sen slope and Mann-Kendall test

The Mann-Kendall trend test was used to analyze the changing trends and significance of VPD and E globally from 1981 to 2020 (Mann, 1945), and the IL-SEN method was used to quantify the magnitudes of the changing trends of the two (Sen, 1968). This method determines the monotonic trend of a sequence by calculating the test statistic S (S 2) and its symbolic function Sgn (formula 3), where β>0 indicates that the sequence has an upward trend (S 1). The significance of the trend is evaluated by the test statistic Z (S 4), and the Z value is calculated based on S and its Var Var (S) (S 5). This method has no strict requirements for the distribution of data and belongs to non-parametric test methods. It has been widely used in the analysis of time series and can well reflect the changes of VPD and E. The equation is as follows:

$$\beta=\mathrm{Median}\left(\frac{x_j-x_i}{j-i}\right) \quad \forall j>i| \tag{1}$$

Median( )represents the calculation of the median value. When β is greater than 0，it indicates an increasing trend in the research subject.

The test statistic S is calculated as follows:

$$S=\sum_{i=1}^{n}\sum_{j=i+1}^{n}\mathrm{sgn}\left(x_j-x_i\right) \tag{2}$$

where Sgn() is the sign function, calculated as:

$$\mathrm{Sgn}\left(x_j-x_i\right)=\begin{cases}1 & x_j-x_i>0\\ 0 & x_j-x_i=0\\ -1 & x_j-x_i<0\end{cases} \tag{3}$$

The trend significance is evaluated using the test statistic Z, which is computed as follows:

$$Z=\begin{cases}\dfrac{S}{\sqrt{\mathrm{Var}(S)}} & S>0\\ 0 & S=0\\ \dfrac{S+1}{\sqrt{\mathrm{Var}(S)}} & S<0\end{cases} \tag{4}$$

https://doi.org/10.5194/egusphere-2025-4820
Preprint. Discussion started: 21 October 2025

where Var (variance) is computed as:

$$\mathrm{Var(S)}=\frac{n(n-1)(2n+5)}{18}. \tag{5}$$

where n represents the number of data points in the sequence.

When the absolute value of Z exceeds specific thresholds (1.64, 1.96, or 2.58), it indicates that the time series passes the significance test at confidence levels of 90%, 95%, and 99%, respectively. Using a two-tailed trend test, the critical value $Z(1-\alpha/2)$ is obtained from the normal distribution table under a given significance level. When $|Z| \leq Z(1-\alpha/2)$, the null hypothesis is accepted, indicating no significant trend; when $|Z| > Z(1-\alpha/2)$, the null hypothesis is rejected, indicating a significant trend.

2.2.2 Estimation of the VPD sensitivity to the E

Due to the complex bidirectional interactions between local background climate and varying E conditions across different scales, this study adopts a moving window strategy inspired by the "space-for-time" approach to calculate the sensitivity of E to VPD (dE/dVPD) (Y. Li et al., 2023). The core assumption is that the target pixel shares the same background climate with neighboring pixels within the moving window, so differences in E between the target and comparison pixels are attributed to biophysical feedbacks induced by land cover changes. Similarly, under certain constraints, we assume VPD is the sole driver of spatial variations in E, allowing the estimation of E sensitivity to VPD through spatially adjacent E and VPD data (Li et al., 2024). The advantage of this method lies in its exclusion of climate natural variability effects on VPD—since pixels with varying VPD values within the moving window share the same background climate.

This study employs the spatial moving window strategy to generate monthly dE/dVPD values (Zhao and Feng, 2024). Specifically, for a given target pixel, all potential comparison samples are selected from neighboring spatial pixels within the moving window, which is set to 5 × 5 km based on previous studies. We further establish screening criteria to exclude the influence of land cover differences: selected pixels must share the same dominant land cover type as the target pixel, with

https://doi.org/10.5194/egusphere-2025-4820
Preprint. Discussion started: 21 October 2025

coverage differences not exceeding 10% according to MODIS land cover data. By regressing the differences in E and VPD between all comparison pixels and the target pixel, the sensitivity for the target pixel is obtained. In this process, the nonparametric Theil–Sen's slope estimator is applied to address potential skewness in the sample distribution.

$$slope=median\left(\frac{y_i-y_j}{x_i-x_j}\right) \quad (6)$$

Here x and y indicate the E and VPD differences; i and j are the geolocations of samples within the moving window. Theil–Sen slope estimator adopts the median value of a range of possible slopes and is thus insensitive to the statistical outliers of the samples.

2.2.3 Pearson Correlation Analysis

The Pearson correlation coefficient is a statistical measure used to assess the relationship between variables, with values ranging from –1 to 1. However, the observed correlation may occur by chance; therefore, the p-value is employed as an indicator of statistical significance (Zhang and Zeng, 2024). In this study, for each pixel, we calculate the Pearson correlation coefficient between the corresponding pixel values of vapor pressure deficit (VPD) and different components of evapotranspiration (Ei, Et, Eb) (Miralles et al., 2011) to quantify the degree of linear association at that location. The correlation coefficient RRR is computed as follows:

$$R=\frac{n\sum x_i y_i-\sum x_i\sum y_i}{\sqrt{n\sum x_i^2-(\sum x_i)^2}\sqrt{n\sum y_i^2-(\sum y_i)^2}} \quad (7)$$

where n denotes the sample size, and x and y represent the time series values of VPD and the respective evapotranspiration components Ei, Et, and Eb. Based on the absolute value of R, correlation strength is categorized into five levels: negligible or no correlation (｜R｜<0.2); weak correlation (0.2 ≤ ｜R｜<0.4); moderate correlation (0.4 ≤ ｜R｜<0.6); strong correlation (0.6 ≤ ｜R｜<0.8); and very strong correlation (0.8 ≤ ｜R｜≤1).

https://doi.org/10.5194/egusphere-2025-4820
Preprint. Discussion started: 21 October 2025

2.2.4 Piecewise Linear Regression and Generalized Additive Model (GAM)

Piecewise linear regression is suited for scenarios where the independent variable exhibits different linear relationships across distinct intervals, allowing simultaneous detection of trends and breakpoints (Yu et al., 2024). GAM are non-parametric regression techniques that capture nonlinear relationships between independent and dependent variables through smoothing functions, where the mean or location parameter of the response variable depends on the sum of smoothing functions of the covariates (Brunner and Naveau, 2023). This study applies these two models to investigate the nonlinear relationship and potential thresholds between VPD and E, and further categorizes the data into five climate zones—tropical (A), arid (B), temperate (C), frigid (D), and polar (E)—as well as into arid versus humid regions, in order to explore regional differences. To ensure data quality, outliers were removed by filtering values outside the 1st and 99th percentiles of VPD and E. Data processing was conducted using Python libraries rasterio and geopandas.To identify thresholds in the VPD–E relationship, piecewise linear regression was applied, modeling VPD as the independent variable and E as the dependent variable with a single breakpoint x_0. The model is defined as:

$$E = \begin{cases} k_1 \cdot \mathrm{VPD} + b_1 & \text{if VPD} < x_0, \\ k_2 \cdot \mathrm{VPD} + (k_1 - k_2) \cdot x_0 + b_1 & \text{if VPD} \geq x_0, \end{cases} \tag{8}$$

where k_1 and k_2 represent the slopes before and after the breakpoint respectively, and b_1 is the intercept. Parameters (x_0,k_1,k_2,b_1) were estimated using scipy.optimize. Model performance was evaluated by the coefficient of determination (R^2) and root mean square error (RMSE).

$$E=f(\mathrm{VPD}) \tag{9}$$

Here, f is a cubic spline function (s(0)). The threshold is determined by calculating the second derivative of the GAM prediction curve to identify the VPD value corresponding to the point with the maximum curvature. The 95% confidence interval is used to assess uncertainty. The model fitting quality was evaluated by R^2

https://doi.org/10.5194/egusphere-2025-4820
Preprint. Discussion started: 21 October 2025

and RMSE.

2.2.5 Quantifying the Influence of VPD on E under Multi-Factor Coupling Using SEM

To elucidate the direct and indirect regulatory mechanisms of VPD on E under the coupling effects of multiple factors, this study employs Structural Equation Modeling (SEM) to model and quantify the path relationships among various variables. SEM, as a multivariate causal analysis tool, is widely utilized in ecohydrological systems to identify and disentangle complex inter-variable relationships, enabling simultaneous estimation of direct effects of multiple independent variables on a dependent variable, indirect effects mediated through intervening variables, and total effects (Guo et al., 2025).

During the model construction process, it is assumed that temperature (T) and precipitation (PRE) have a direct impact on VPD. Meanwhile, T, PRE, and VPD regulate soil moisture (SM) and leaf area index (LAI). Ultimately, VPD, SM, and LAI jointly affect E. The model data is based on multi-source remote sensing and reanalysis products from 1981 to 2020. All variables were standardized and included in the analysis.

We use the "piecewiseSEM" package to build the path model and extract the standardized path coefficient (Std.Estimate) through the "coefs" function. Further utilize the path coefficients to calculate the indirect effects of each factor on E, and superimpose the direct paths to obtain the total effect. The model fit degree was evaluated using Fisher's C statistics and AIC (Jing et al., 2015).

3. Results

3.1 Spatiotemporal Distribution Characteristics of VPD and E

From 1981 to 2020 (Fig. 1a), global VPD exhibited a significant upward trend accompanied by strong spatial heterogeneity. Regions with statistically significant increases accounted for 76.22% of the terrestrial surface, with particularly pronounced increases in arid and semi-arid zones, reflecting the global intensification of atmospheric aridification. Seasonally (Fig. 1c), VPD showed a distinct annual cycle, peaking in summer (typically July) and reaching a minimum in winter, indicating that

https://doi.org/10.5194/egusphere-2025-4820
Preprint. Discussion started: 21 October 2025

it is jointly regulated by meteorological drivers such as air temperature and evaporative demand.

During the same period, global terrestrial E also displayed an overall increasing trend (Fig. 1b), with significant growth concentrated in East Asia and Northern Europe, whereas notable declines were detected in Africa, central South America, southwestern North America, and eastern Australia. At the seasonal scale (Fig. 1d), the peak of E generally occurred in June, preceding that of VPD by about one month, suggesting an earlier hydrological response to atmospheric conditions. This shift is likely associated with abundant soil moisture in spring and the advancement of vegetation phenology. Further analyses revealed that in regions with rising VPD, E exhibited a clear decreasing tendency, highlighting the suppressive effect of intensified atmospheric aridity on land surface water fluxes, particularly in water-limited areas where soil–vegetation regulation is weak. In contrast, at higher latitudes where VPD declined or increased only slightly, E generally rose, likely driven by synergistic effects of rising temperatures, extended frost-free periods, and strengthened growing-season vegetation activity.

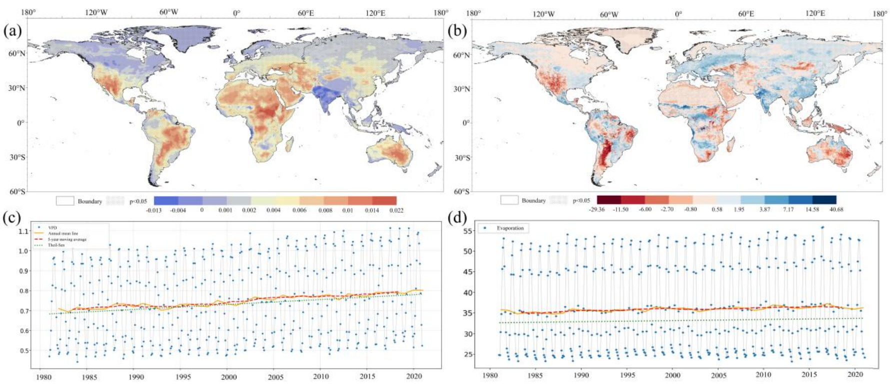

Figure 1. Spatiotemporal distribution characteristics of VPD and E: (a) VPD trend characteristics; (b) E trend characteristics; (c) monthly variation of VPD; (d) monthly variation of E.

3.2 Global-scale Terrestrial E Response to VPD

At the global scale, the interannual response of E to VPD shows clear and uneven spatial patterns (Fig. 2a). Approximately 60.71% of terrestrial areas exhibit

https://doi.org/10.5194/egusphere-2025-4820
Preprint. Discussion started: 21 October 2025

positive sensitivity to rising VPD, whereas 39.29% show negative sensitivity, with a global mean sensitivity of 293.27 ± 62.28 mm·hPa⁻¹·yr⁻¹ (Fig. 2a). From a climatic perspective, arid and cold regions are more prone to negative responses, because in these areas VPD-driven surface water fluxes are constrained either by limited water availability or by insufficient energy, resulting in suppressive effects. By contrast, in regions with higher temperature or precipitation, the positive response of E to VPD becomes stronger (Fig. 2b). For typical water-limited regions such as western Australia and southern Africa, increases in VPD are accompanied by declines in E, reflecting a stomatal closure feedback that reduces water loss and dampens evapotranspiration.

Across land-use types, we grouped 16 categories into four major classes: forest, grassland and wetland, cropland, and barren land (Fig. 2c). All classes generally show positive sensitivity to VPD, but with marked differences in magnitude: forests respond the most strongly (405.34 mm·hPa⁻¹·yr⁻¹), followed by grasslands and wetlands (342.26 mm·hPa⁻¹·yr⁻¹) and barren areas (200.40 mm·hPa⁻¹·yr⁻¹), whereas croplands display the weakest sensitivity (78.12 mm·hPa⁻¹·yr⁻¹). Taken together, these results indicate that in regions with dense vegetation cover, higher VPD is more likely to stimulate E, while in sparsely vegetated or managed cropland areas, the effect remains comparatively limited.

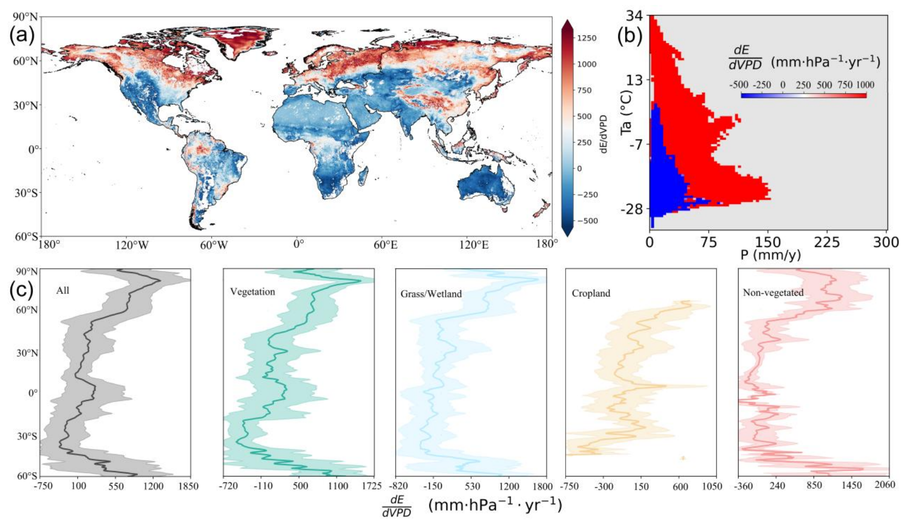

https://doi.org/10.5194/egusphere-2025-4820
Preprint. Discussion started: 21 October 2025

Figure 2. Response of E to VPD during the study period (1981–2020): (a) spatial distribution of sensitivity; (b) variation of sensitivity indicating differences across climate zones, which are delineated based on annual precipitation (P, x-axis) and air temperature (Ta, y-axis); (c) latitudinal distribution of dE/dVPD across different underlying surface types, with shaded areas representing the standard deviation of latitude.

3.3 Global Pattern of the Relationship between VPD and Et, Ei, and Eb

From 1981 to 1997, E showed pronounced interannual variability but still followed an overall upward trend, with the global annual mean increasing by 1.47 mm/yr (Fig. 3a). Following the strong El Niño event in 1998, this upward trend weakened, shifted into a decline around 2008, and then rebounded under the influence of the 2009 La Niña event. Satellite observations (Fig. 3b) confirm this dynamic: VPD rose abruptly in 1998 (0.034 hPa yr^{-1}), dropped temporarily, and then peaked at 7.839 hPa in 2010. The correlation between E and VPD at the decadal scale suggests that the intensification and alleviation of atmospheric aridification correspond to the suppression and recovery of E, respectively.

At the spatial scale, correlations between VPD and different E components display broadly consistent geographic patterns (Fig. 3d, f, h), though with varying magnitudes: VPD has the strongest influence on Et ($r = 0.66$), followed by Ei ($r = 0.37$), while Eb exhibits an overall negative correlation ($r = –0.15$) (Fig. 3c). In high-latitude regions and parts of the low latitudes, VPD significantly enhances E, with its effect on Et being particularly prominent compared to Eb and Ei. This occurs because higher VPD increases atmospheric demand for water vapor, directly driving diffusion from leaves through stomata into the atmosphere and thereby stimulating transpiration. Conversely, in arid and semi-arid regions at mid- and low latitudes (e.g., central Australia and southern Africa), intensified atmospheric aridification leads to negative correlations between VPD and both Ei and Eb (Fig. 3f, h), reflecting suppressed canopy interception and soil evaporation. Across temporal scales, Et consistently shows the strongest interannual coherence with VPD, followed by Eb, whereas Ei responds the weakest (Fig. 3e, g, i), consistent with the above spatial

https://doi.org/10.5194/egusphere-2025-4820
Preprint. Discussion started: 21 October 2025

analyses.

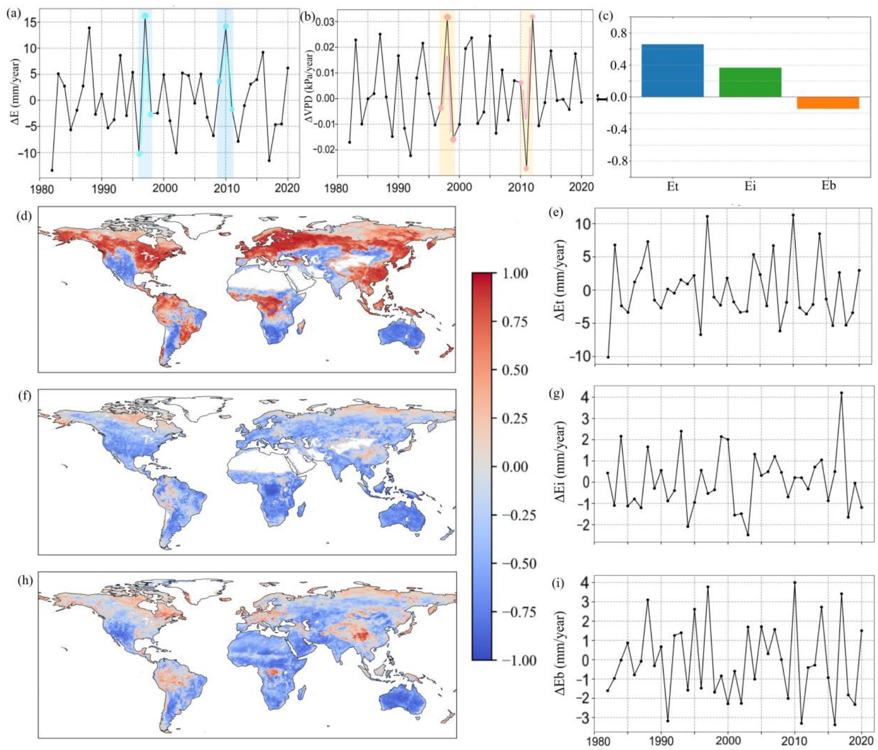

Figure 3. Global influence of VPD on different E components. (a, b) Interannual fluctuations of E and VPD, respectively; (c) Pearson correlation coefficients (r) between VPD and Et, Ei, and Eb; (d, f, h) spatial distribution of Pearson correlations between VPD and Et, Ei, and Eb computed using annual data from 1981 to 2020; (e, g, i) interannual variations of Et, Ei, and Eb, respectively.

4 Discussion、

4.1 Threshold effect and the universality of nonlinearity

This study reveals a widespread nonlinear relationship between E and VPD, indicating that terrestrial ecosystems generally exhibit threshold-like responses to VPD variability. Based on piecewise linear regression and GAM, we quantified VPD thresholds across different climate zones. The results show a clear climatic gradient in thresholds (Fig. 4a–e): tropical (0.79 kPa) > temperate (0.68 kPa) > cold (0.28 kPa) > polar (0.07 kPa), and arid (1.31 kPa) > humid (0.32 kPa). The high consistency

https://doi.org/10.5194/egusphere-2025-4820
Preprint. Discussion started: 21 October 2025

between the two models (Fig. 4f, i) confirms the robustness of these thresholds and reveals pronounced regional differences in E's response to VPD. Notably, the low threshold (0.07–0.08 kPa) in polar zones suggests that even slight increases in VPD can induce substantial changes in E, whereas the high threshold (1.67–1.68 kPa) in temperate zones likely reflects vegetation adaptation to long-term arid conditions (Gao et al., 2024; Lian et al., 2021). These results underscore the key regulatory roles of climatic background and ecosystem traits in shaping VPD thresholds.

Model comparisons demonstrate that GAM outperforms piecewise regression in capturing nonlinear responses, especially in the cold climate zone ($R^2 = 0.93$; Fig. 4d) and humid regions ($R^2 = 0.91$). This finding is further supported by the cross-zone threshold analysis (Fig. 4f). Quantitatively identifying VPD thresholds is essential for predicting ecosystem responses to intensified atmospheric aridification under future climate change (Li et al., 2020). Regions with lower thresholds (e.g., cold and polar zones) are more vulnerable to VPD increases, facing earlier risks of water stress and associated declines in vegetation productivity and carbon cycling. To better uncover the underlying mechanisms, future studies should integrate multi-source ecohydrological factors, particularly in regions with relatively weak model performance, such as tropical zones (GAM $R^2 = 0.25$; Fig. 4a), thereby improving both the precision of threshold detection and its ecological interpretability.

https://doi.org/10.5194/egusphere-2025-4820
Preprint. Discussion started: 21 October 2025

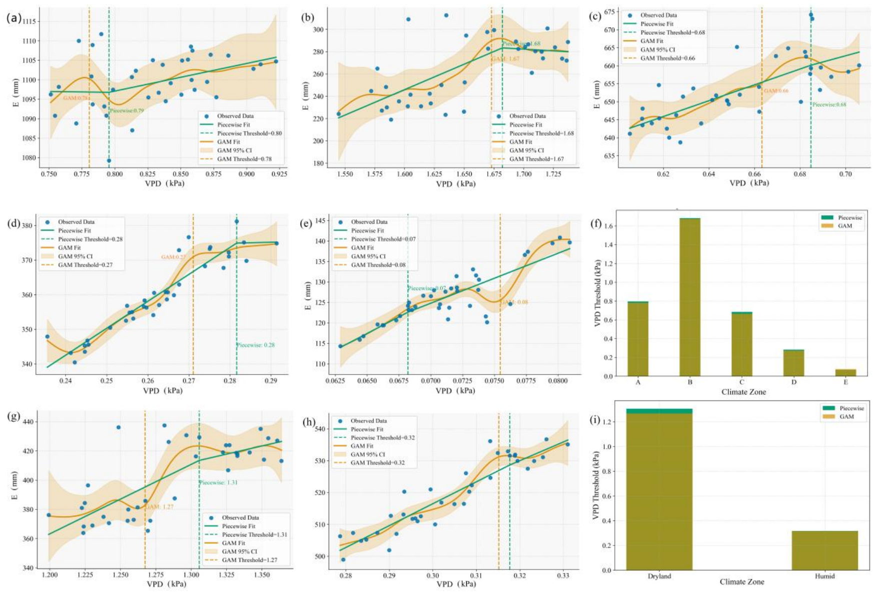

Figure 4. Nonlinear relationships between VPD and E across different climate zones: tropical (a), arid (b), temperate (c), cold (d), and polar (e). Panels (f) and (g) show results for arid and humid regions, respectively. The plots display observed data points, piecewise linear regression fits (red solid lines), GAM fits (green solid lines), and their corresponding thresholds (dashed lines). Panels (h) and (i) compare the thresholds derived from piecewise regression and GAM across climate zones (h) and between arid/humid regions (i) using bar charts.

4.2 Mechanism of VPD regulating E under multi-factor coupling

This study employed SEM to quantitatively reveal the complex mechanisms by which VPD regulates global terrestrial E under multi-factor coupling, with all factors jointly explaining 77% of the variance in E (Fig. 5a). T exerts a significant positive effect on VPD (standardized coefficient = 0.58), whereas Pre has a significant negative effect (standardized coefficient = –0.40), indicating that sufficient water supply can effectively reduce VPD. Meanwhile, the strong negative relationship between SM and VPD (standardized coefficient = –0.84) suggests that under high VPD conditions, SM is rapidly depleted, potentially leading to substantial alterations in ecosystem water budgets (Liu et al., 2019). Previous studies have shown that the response of Et to VPD varies with environmental and plant traits: in water-limited

https://doi.org/10.5194/egusphere-2025-4820
Preprint. Discussion started: 21 October 2025

regions, reduced SM may suppress Et, whereas in moisture-abundant regions, Et may rise with increasing VPD (Massmann et al., 2019). Our SEM results are consistent with this understanding, highlighting that the interaction between VPD and SM represents a critical regulatory pathway for E. Moreover, LAI increases markedly under high VPD conditions (standardized coefficient = 0.90), but its direct effect on Et remains weak (standardized coefficient = 0.07), suggesting that VPD primarily influences Et indirectly by modulating vegetation status and SM, thereby regulating E. This indirect pathway aligns with the consensus in ecohydrology: VPD influences stomatal conductance, thereby indirectly controlling photosynthesis and transpiration, and ultimately shaping E dynamics (Zhang et al., 2023).

Within the multi-factor coupling framework, VPD exerts a significant direct effect on E (direct effect coefficient = 0.5443) while also amplifying its indirect effect via its positive influence on LAI; the contributions of T and PRE to E are also pronounced (Fig. 5b). These results underscore the interactive coupling pathways between VPD and other climatic drivers, particularly the mechanism by which VPD indirectly regulates E through vegetation structural adjustments. With ongoing climate change driving rising temperatures and shifting precipitation regimes, VPD is projected to increase continuously throughout the 21st century (Yuan et al., 2019). This trajectory will impose major challenges on global ecosystems, especially those constrained by water availability. Our SEM findings highlight the importance of systematically accounting for the interactions and feedbacks among VPD, T, PRE, SM, and LAI when developing adaptation strategies and refining predictive models. Future work should further explore regional heterogeneity and the long-term adaptive strategies of vegetation to enhance the predictive accuracy of global ecohydrological models.

https://doi.org/10.5194/egusphere-2025-4820
Preprint. Discussion started: 21 October 2025

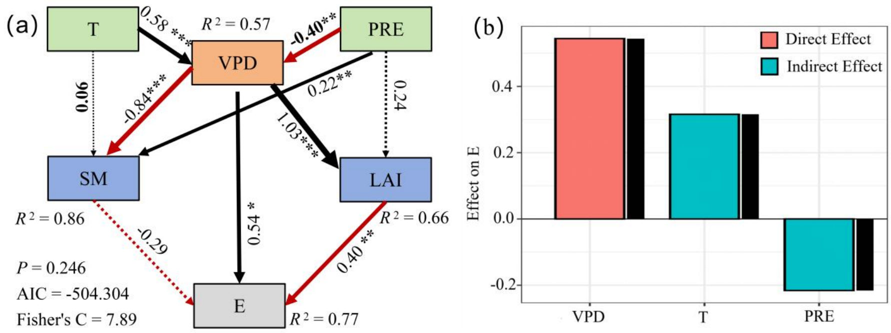

Figure 5. Direct and indirect effects of T, PRE, SM, LAI, and VPD on E. Numbers adjacent to the arrows represent standardized path coefficients indicating the strength of the relationships. Arrow widths are proportional to the magnitude of the standardized coefficients. Significant paths are marked with asterisks. The p-value and Chi-square test statistic are shown in the lower-left corner of the model.

4.3 Implications of land-atmosphere feedback under future VPD increase scenarios

The anticipated rise in VPD will continuously reshape land–atmosphere interactions by regulating E, thereby profoundly influencing both regional and global water cycle patterns (Yuan et al., 2019). In arid regions, when VPD exceeds the critical threshold (1.67–1.68 kPa; Fig. 4f), E is substantially suppressed (Fig. 4b, f), triggering a positive “SM–atmospheric water vapor” feedback loop: declining SM reduces E, weakens atmospheric water vapor flux, suppresses cloud formation and precipitation, and further intensifies regional drought (Zhou et al., 2019). In humid regions, E may initially rise with increasing VPD in the short term (Fig. 2a); however, as available water becomes progressively depleted, this enhancement effect may weaken or even reverse, disrupting cross-regional water vapor transport and precipitation recycling. Responses to elevated VPD vary considerably across climate zones and vegetation types. Forest ecosystems are generally highly sensitive to VPD anomalies, where VPD-induced water stress can markedly reduce productivity and elevate the risks of tree mortality and forest degradation (Will et al., 2013). In contrast, agricultural systems may alleviate some negative impacts of increasing VPD through irrigation, but in water-scarce regions this buffering capacity is constrained,

https://doi.org/10.5194/egusphere-2025-4820
Preprint. Discussion started: 21 October 2025

potentially amplifying the instability of agricultural yields.

Overall, the continuous rise in VPD may intensify land–atmosphere feedbacks and magnify uncertainties in global water and carbon cycles (Gentine et al., 2019). This underscores the urgent need to refine climate models to better capture regional heterogeneity in ecosystem responses. For ecologically fragile regions—particularly polar, frigid, and arid zones—developing targeted water resource management and ecological conservation strategies is essential to enhance ecosystem adaptability and resilience, thereby mitigating ecological risks and climate feedbacks associated with rising VPD.

4.4 Uncertainty and future outlook

This research provides a new perspective for understanding the mechanisms by which global VPD regulates E, yet three major sources of uncertainty remain. In terms of data, this study relies on ERA5 reanalysis data for statistical analysis. Although ERA5 incorporates higher-quality near-surface meteorological inputs, it still exhibits systematic deviations from in situ observations. For example, ERA5 tends to overestimate SM in arid regions (Kokkalis et al., 2024), which may dampen the statistical significance of the VPD–SM–ET pathway. To improve the robustness of the findings, future work should utilize multi-source datasets at different temporal scales to more accurately evaluate the impact of VPD on E. In terms of environmental factors, although multiple drivers were considered when examining the VPD–E relationship, the legacy effects of climatic factors on terrestrial ecosystems (Miralles et al., 2014) introduce additional uncertainty. Future studies should incorporate a broader suite of environmental variables and ecological processes and investigate their interactive effects with VPD and E, thereby providing a more comprehensive understanding of the global land–atmosphere coupling system. In terms of methodology, this study applied piecewise linear regression and GAM to quantify the nonlinear relationship between VPD and E. However, these approaches rely on simplifying assumptions that may bias results. For instance, piecewise regression assumes a single breakpoint in the VPD–E relationship, whereas the actual relationship may involve multiple thresholds or gradual nonlinear transitions.

https://doi.org/10.5194/egusphere-2025-4820
Preprint. Discussion started: 21 October 2025

Moreover, in tropical regions, the GAM fit was relatively weak ($R^2 = 0.25$; Fig. 4a), possibly due to data noise or suboptimal parameter selection. Future studies should validate thresholds using FLUXNET site-level observations and adopt more advanced approaches, such as improved GAM formulations or machine learning techniques, to capture the inherently complex nonlinear dynamics.

5 Conclusion

This study integrates multi-source remote sensing and reanalysis data from 1981 to 2020 to systematically evaluate the pathways and regional heterogeneity through which VPD influences global terrestrial E and its components (Et, Ei, Eb). The results show that global VPD has increased significantly (covering 76.22% of land areas). Overall, E exhibits an increasing trend, but in regions where VPD rises rapidly, E decreases markedly. This essentially reflects the mismatch between limited water supply and surging atmospheric demand, which triggers stomatal closure in plants and soil water limitation, thereby suppressing water fluxes. The global mean sensitivity of E to VPD is 293.27 ± 62.28 mm·hPa^{-1}·yr^{-1}, dominated by positive responses (60.71%) and stronger in regions with higher vegetation cover, whereas 39.29% of regions exhibit negative sensitivity. Clear nonlinear relationships and threshold gradients are evident: thresholds by aridity range from 1.31 kPa in arid zones to 0.32 kPa in humid zones, and by climate zones from 1.68 kPa in arid, 0.79 kPa in tropical, 0.68 kPa in temperate, 0.28 kPa in frigid, to 0.07 kPa in polar climates. Model fits are stronger in frigid ($R^2 = 0.93$) and humid ($R^2 = 0.86$) zones. At the component level, Et is most sensitive to VPD ($r = 0.66$) and exerts a positive influence on E, whereas in mid-latitude arid–semiarid regions, VPD suppresses Ei and Eb, indicating the constraint of atmospheric dryness on non-transpiration components under water-limited conditions. Structural equation modeling further reveals that multiple drivers jointly explain 77% of the variance in E. VPD exerts a strong direct effect (direct effect coefficient = 0.5443) and indirectly amplifies its influence through its positive regulation of LAI along the VPD–LAI–E pathway. Overall, the continued rise in VPD under global warming may reshape the allocation of terrestrial energy and

https://doi.org/10.5194/egusphere-2025-4820
Preprint. Discussion started: 21 October 2025

water, intensify land–atmosphere feedbacks, and exacerbate regional hydroclimatic divergence. While this study provides quantitative constraints and mechanistic insights for future predictions of the water cycle and water resource management, three major uncertainties remain: the representation of lagged and cumulative effects, the estimation of Ei and Eb, and the identification of nonlinear thresholds. Future work should incorporate high-resolution observations, isotope tracing, and experimental evidence to refine understanding of the regulatory mechanisms of VPD on E.

Data availability

The GLEAM v4.2a evapotranspiration product used in this study is available at https://www.gleam.eu/. ERA5 reanalysis data, including VPD, air temperature, dew point temperature, soil moisture, solar radiation, and precipitation, can be obtained from https://www.ecmwf.int/en/forecasts/dataset/ecmwf-reanalysis-v5. The MCD12C1 v6.1 land use product is available through the Google Earth Engine platform (https://earthengine.google.com/). Climate zones are derived from the updated Köppen–Geiger classification and aridity index data . The GIMMS LAI V1.2 dataset is available from https://ecocast.arc.nasa.gov/data/pub/gimms/LAI/. All data used in this study are publicly accessible or available from the corresponding references.

Code availability

The code used for data processing and analysis in this study is available from the corresponding author upon reasonable request.

Author contributions statement

Yuxin Miao: Writing-Original draft preparation; Guofeng Zhu: Writing-Reviewing and Editing; Yuhao Wang: Data curation; Enwei Huang: Methodology; Qingyang Wang: Visualization; Yani Gun: Investigation; Zhijie Zheng: Supervision; Jiangwei Yang: Software; Wenmin Li: Validation; Ziwen Liu: Software;

https://doi.org/10.5194/egusphere-2025-4820
Preprint. Discussion started: 21 October 2025

Competing interests

The authors declare that they have no conflict of interest.

Acknowledgements

This research was financially supported by the National Natural Science Foundation of China (42371040), the Western Light Young Scholars Program of the Chinese Academy of Sciences(25JR6KA001), the Key Natural Science Foundation of Gansu Province (23JRRA698), the Key Research and Development Program of Gansu Province (22YF7NA122), the Cultivation Program of Major key projects of Northwest Normal University (NWNU-LKZD-202302), the Oasis Scientific Research achievements Breakthrough Action Plan Project of Northwest normal University (NWNU-LZKX-202303).

References

Brunner, M.I., Naveau, P., 2023. Spatial variability in Alpine reservoir regulation: deriving reservoir operations from streamflow using generalized additive models. Hydrol. Earth Syst. Sci. 27, 673–687. https://doi.org/10.5194/hess-27-673-2023

Cao, S., Li, M., Zhu, Z., Wang, Z., Zha, J., Zhao, W., Duanmu, Z., Chen, J., Zheng, Y., Chen, Y., Myneni, R.B., Piao, S., 2023. Spatiotemporally consistent global dataset of the GIMMS leaf area index (GIMMS LAI4g) from 1982 to 2020. Earth Syst. Sci. Data 15, 4877–4899. https://doi.org/10.5194/essd-15-4877-2023

Chai, Y., Yue, Y., Slater, L., Miao, C., 2025. Emergent constraints indicate slower increases in future global evapotranspiration. npj Clim Atmos Sci 8, 46. https://doi.org/10.1038/s41612-025-00932-1

Chen, N., Zhang, Y., Yuan, F., Song, C., Xu, M., Wang, Q., Hao, G., Bao, T., Zuo, Y., Liu, J., Zhang, T., Song, Y., Sun, L., Guo, Y., Zhang, H., Ma, G., Du, Y., Xu, X., Wang, X., 2023. Warming-induced vapor pressure deficit suppression of vegetation growth diminished in northern peatlands. Nat Commun 14, 7885.

https://doi.org/10.1038/s41467-023-42932-w

Copernicus Climate Change Service, 2019. ERA5-Land monthly averaged data from 1950 to present. https://doi.org/10.24381/CDS.68D2BB30

Friedl, M., Sulla-Menashe, D., 2022. MODIS/Terra+Aqua Land Cover Type Yearly L3 Global 0.05Deg CMG V061. https://doi.org/10.5067/MODIS/MCD12C1.061

Gao, X., Zhuo, W., Gonsamo, A., 2024. Humid, Warm and Treed Ecosystems Show Longer Time-Lag of Vegetation Response to Climate. Geophysical Research Letters 51, e2024GL111737. https://doi.org/10.1029/2024GL111737

Gentine, P., Green, J.K., Guérin, M., Humphrey, V., Seneviratne, S.I., Zhang, Y., Zhou, S., 2019. Coupling between the terrestrial carbon and water cycles—a review. Environ. Res. Lett. 14, 083003. https://doi.org/10.1088/1748-9326/ab22d6

Guo, M., Yang, L., Zhang, L., Shen, F., Meadows, M.E., Zhou, C., 2025. Hydrology, vegetation, and soil properties as key drivers of soil organic carbon in coastal wetlands: A high-resolution study. Environmental Science and Ecotechnology 23, 100482. https://doi.org/10.1016/j.ese.2024.100482

Hermann, M., Wernli, H., Röthlisberger, M., 2024. Drastic increase in the magnitude of very rare summer-mean vapor pressure deficit extremes. Nat Commun 15, 7022. https://doi.org/10.1038/s41467-024-51305-w

Hsu, H., Dirmeyer, P.A., 2021. Nonlinearity and Multivariate Dependencies in the Terrestrial Leg of Land-Atmosphere Coupling. Water Resources Research 57, e2020WR028179. https://doi.org/10.1029/2020WR028179

Jing, X., Sanders, N.J., Shi, Yu, Chu, H., Classen, A.T., Zhao, K., Chen, L., Shi, Yue, Jiang, Y., He, J.-S., 2015. The links between ecosystem multifunctionality and above- and belowground biodiversity are mediated by climate. Nat Commun 6, 8159. https://doi.org/10.1038/ncomms9159

Kim, Y., Johnson, M.S., 2025. Deciphering the role of evapotranspiration in declining relative humidity trends over land. Commun Earth Environ 6, 105. https://doi.org/10.1038/s43247-025-02076-9

Kokkalis, P., Al Jassar, H.K., Al Sarraf, H., Nair, R., Al Hendi, H., 2024. Evaluation of

ERA5 and NCEP reanalysis climate models for precipitation and soil moisture over a semi-arid area in Kuwait. Clim Dyn 62, 4893–4904. https://doi.org/10.1007/s00382-024-07141-1

Kumagai, T., Yoshifuji, N., Tanaka, N., Suzuki, M., Kume, T., 2009. Comparison of soil moisture dynamics between a tropical rain forest and a tropical seasonal forest in Southeast Asia: Impact of seasonal and year-to-year variations in rainfall. Water Resources Research 45, 2008WR007307. https://doi.org/10.1029/2008WR007307

Lebrija-Trejos, E., Hernández, A., Wright, S.J., 2023. Effects of moisture and density-dependent interactions on tropical tree diversity. Nature 615, 100–104. https://doi.org/10.1038/s41586-023-05717-1

Li, F., Xiao, J., Chen, J., Ballantyne, A., Jin, K., Li, B., Abraha, M., John, R., 2023. Global water use efficiency saturation due to increased vapor pressure deficit. Science 381, 672–677. https://doi.org/10.1126/science.adf5041

Li, K., Tong, Z., Liu, X., Zhang, J., Tong, S., 2020. Quantitative assessment and driving force analysis of vegetation drought risk to climate change:Methodology and application in Northeast China. Agricultural and Forest Meteorology 282–283, 107865. https://doi.org/10.1016/j.agrformet.2019.107865

Li, T., He, B., Chen, D., Chen, H.W., Guo, L., Yuan, W., Fang, K., Shi, F., Liu, L., Zheng, H., Huang, L., Wu, X., Hao, X., Zhao, X., Jiang, W., 2024. Increasing Sensitivity of Tree Radial Growth to Precipitation. Geophysical Research Letters 51, e2024GL110003. https://doi.org/10.1029/2024GL110003

Li, Y., Li, Z.-L., Wu, H., Zhou, C., Liu, X., Leng, P., Yang, P., Wu, W., Tang, R., Shang, G.-F., Ma, L., 2023. Biophysical impacts of earth greening can substantially mitigate regional land surface temperature warming. Nat Commun 14, 121. https://doi.org/10.1038/s41467-023-35799-4

Lian, X., Piao, S., Chen, A., Huntingford, C., Fu, B., Li, L.Z.X., Huang, J., Sheffield, J., Berg, A.M., Keenan, T.F., McVicar, T.R., Wada, Y., Wang, X., Wang, T., Yang, Y., Roderick, M.L., 2021. Multifaceted characteristics of dryland aridity changes in a warming world. Nat Rev Earth Environ 2, 232–250. https://doi.org/10.1038/s43017-021-00144-0

Liu, H., Gleason, S.M., Hao, G., Hua, L., He, P., Goldstein, G., Ye, Q., 2019. Hydraulic traits are coordinated with maximum plant height at the global scale. Sci. Adv. 5, eaav1332. https://doi.org/10.1126/sciadv.aav1332

Mann, H.B., 1945. Nonparametric Tests Against Trend. Econometrica 13, 245. https://doi.org/10.2307/1907187

Massmann, A., Gentine, P., Lin, C., 2019. When Does Vapor Pressure Deficit Drive or Reduce Evapotranspiration? J Adv Model Earth Syst 11, 3305–3320. https://doi.org/10.1029/2019MS001790

Miner, G.L., Bauerle, W.L., Baldocchi, D.D., 2017. Estimating the sensitivity of stomatal conductance to photosynthesis: a review. Plant Cell & Environment 40, 1214–1238. https://doi.org/10.1111/pce.12871

Miralles, D.G., Bonte, O., Koppa, A., Baez-Villanueva, O.M., Tronquo, E., Zhong, F., Beck, H.E., Hulsman, P., Dorigo, W., Verhoest, N.E.C., Haghdoost, S., 2025. GLEAM4: global land evaporation and soil moisture dataset at 0.1° resolution from 1980 to near present. Sci Data 12, 416. https://doi.org/10.1038/s41597-025-04610-y

Miralles, D.G., De Jeu, R.A.M., Gash, J.H., Holmes, T.R.H., Dolman, A.J., 2011. Magnitude and variability of land evaporation and its components at the global scale. Hydrol. Earth Syst. Sci. 15, 967–981. https://doi.org/10.5194/hess-15-967-2011

Miralles, D.G., Van Den Berg, M.J., Gash, J.H., Parinussa, R.M., De Jeu, R.A.M., Beck, H.E., Holmes, T.R.H., Jiménez, C., Verhoest, N.E.C., Dorigo, W.A., Teuling, A.J., Johannes Dolman, A., 2014. El Niño–La Niña cycle and recent trends in continental evaporation. Nature Clim Change 4, 122–126. https://doi.org/10.1038/nclimate2068

Peters, W., Van Der Velde, I.R., Van Schaik, E., Miller, J.B., Ciais, P., Duarte, H.F., Van Der Laan-Luijkx, I.T., Van Der Molen, M.K., Scholze, M., Schaefer, K., Vidale, P.L., Verhoef, A., Wårlind, D., Zhu, D., Tans, P.P., Vaughn, B., White,

https://doi.org/10.5194/egusphere-2025-4820
Preprint. Discussion started: 21 October 2025

J.W.C., 2018. Increased water-use efficiency and reduced CO2 uptake by plants during droughts at a continental scale. Nature Geosci 11, 744–748. https://doi.org/10.1038/s41561-018-0212-7

Rubel, F., Brugger, K., Haslinger, K., Auer, I., 2017. The climate of the European Alps: Shift of very high resolution Köppen-Geiger climate zones 1800–2100. metz 26, 115–125. https://doi.org/10.1127/metz/2016/0816

Rohde, M.M., Albano, C.M., Huggins, X. et al. Groundwater-dependent ecosystem map exposes global dryland protection needs. Nature 632, 101–107 (2024). https://doi.org/10.1038/s41586-024-07702-8

Sen, P.K., 1968. Estimates of the Regression Coefficient Based on Kendall's Tau. Journal of the American Statistical Association 63, 1379–1389. https://doi.org/10.1080/01621459.1968.10480934

Shih, C.-H., Jang, Y.-S., Yang, T.-Y., Huang, C.-Y., Juang, J.-Y., Lo, M.-H., 2025. Impact of diurnal temperature and relative humidity hysteresis on atmospheric dryness in changing climates. Sci. Adv. 11, eadu5713. https://doi.org/10.1126/sciadv.adu5713

Wang, J., Niu, H., Zhang, S., Chen, X., Xia, X., Zhang, Y., Lu, X., He, B., Wu, T., Song, C., Fu, Z., Yao, J., Yuan, W., 2025. Higher warming rate in global arid regions driven by decreased ecosystem latent heat under rising vapor pressure deficit from 1981 to 2022. Agricultural and Forest Meteorology 371, 110622. https://doi.org/10.1016/j.agrformet.2025.110622

Will, R.E., Wilson, S.M., Zou, C.B., Hennessey, T.C., 2013. Increased vapor pressure deficit due to higher temperature leads to greater transpiration and faster mortality during drought for tree seedlings common to the forest–grassland ecotone. New Phytologist 200, 366–374. https://doi.org/10.1111/nph.12321

Yu, H., Xiao, H., Gu, X., 2024. Integrating species distribution and piecewise linear regression model to identify functional connectivity thresholds to delimit urban ecological corridors. Computers, Environment and Urban Systems 113, 102177. https://doi.org/10.1016/j.compenvurbsys.2024.102177

Yuan, W., Zheng, Y., Piao, S., Ciais, P., Lombardozzi, D., Wang, Y., Ryu, Y., Chen, G.,

https://doi.org/10.5194/egusphere-2025-4820
Preprint. Discussion started: 21 October 2025

Dong, W., Hu, Z., Jain, A.K., Jiang, C., Kato, E., Li, S., Lienert, S., Liu, S., Nabel, J.E.M.S., Qin, Z., Quine, T., Sitch, S., Smith, W.K., Wang, F., Wu, C., Xiao, Z., Yang, S., 2019. Increased atmospheric vapor pressure deficit reduces global vegetation growth. Sci. Adv. 5, eaax1396. https://doi.org/10.1126/sciadv.aax1396

Zhang, Q., Manzoni, S., Katul, G., Porporato, A., Yang, D., 2014. The hysteretic evapotranspiration—Vapor pressure deficit relation. JGR Biogeosciences 119, 125–140. https://doi.org/10.1002/2013JG002484

Zhang, W., Koch, J., Wei, F., Zeng, Z., Fang, Z., Fensholt, R., 2023. Soil Moisture and Atmospheric Aridity Impact Spatio-Temporal Changes in Evapotranspiration at a Global Scale. JGR Atmospheres 128, e2022JD038046. https://doi.org/10.1029/2022JD038046

Zhang, W., Zeng, H., 2024. Spatial differentiation characteristics and influencing factors of the green view index in urban areas based on street view images: A case study of Futian District, Shenzhen, China. Urban Forestry & Urban Greening 93, 128219. https://doi.org/10.1016/j.ufug.2024.128219

Zhao, Y., Feng, Q., 2024. Identifying spatial and temporal dynamics and driving factors of cultivated land fragmentation in Shaanxi province. Agricultural Systems 217, 103948. https://doi.org/10.1016/j.agsy.2024.103948

Zhong, Z., He, B., Wang, Y.-P., Chen, H.W., Chen, D., Fu, Y.H., Chen, Y., Guo, L., Deng, Y., Huang, L., Yuan, W., Hao, X., Tang, R., Liu, H., Sun, L., Xie, X., Zhang, Y., 2023. Disentangling the effects of vapor pressure deficit on northern terrestrial vegetation productivity. Sci. Adv. 9, eadf3166. https://doi.org/10.1126/sciadv.adf3166

Zhou, S., Williams, A.P., Berg, A.M., Cook, B.I., Zhang, Y., Hagemann, S., Lorenz, R., Seneviratne, S.I., Gentine, P., 2019. Land–atmosphere feedbacks exacerbate concurrent soil drought and atmospheric aridity. Proc. Natl. Acad. Sci. U.S.A. 116, 18848–18853. https://doi.org/10.1073/pnas.1904955116

Zhuang, Y., Fu, R., Santer, B.D., Dickinson, R.E., Hall, A., 2021. Quantifying contributions of natural variability and anthropogenic forcings on increased

https://doi.org/10.5194/egusphere-2025-4820
Preprint. Discussion started: 21 October 2025

fire weather risk over the western United States. Proc. Natl. Acad. Sci. U.S.A. 118, e2111875118. https://doi.org/10.1073/pnas.2111875118